

Eur. Phys. J. Special Topics **162**, 259–265 (2008)
© EDP Sciences, Springer-Verlag 2008
DOI: 10.1140/epjst/e2008-00801-1

**THE EUROPEAN
PHYSICAL JOURNAL
SPECIAL TOPICS**

RHIC polarimetry

I. Nakagawa^{1,2,a}, I. Alekseev³, A. Bazilevsky⁴, A. Bravar⁵, G. Bunce^{2,4}, S. Dhawan⁶, K.O. Eysler⁷, R. Gill⁴, W. Haeblerli⁸, H. Huang⁴, Y. Makdisi⁴, A. Nass⁹, H. Okada⁴, E. Stephenson¹⁰, D.N. Svirida³, T. Wise⁸, J. Wood⁴, K. Yip⁴, and A. Zelenski⁴

¹ RIKEN, 2-1 Hirosawa Wako, Saitama 351-0198, Japan

² RIKEN-BNL Research Center, Upton, NY 11973, USA

³ Institute for Theoretical and Experimental Physics (ITEP), 117259 Moscow, Russia

⁴ Brookhaven National Laboratory, Upton, NY 11973, USA

⁵ University of Geneva, 1205 Geneva, Switzerland

⁶ Yale University, New Haven, CT 06520, USA

⁷ University of California, Riverside, CA 92521, USA

⁸ University of Wisconsin, WI 53706, USA

⁹ University of Erlangen, 91058 Erlangen, Germany

¹⁰ Indiana University Cyclotron Facility, Bloomington, IN 47408, USA

Abstract. Polarimeters were developed to measure the polarization of the proton beam at RHIC in relative scale through the asymmetry measurement of the elastic proton-carbon scattering. Recoil carbon ions with kinetic energy of $400 \leq E \leq 900$ keV were detected by silicon strip detectors installed at 90° with respect to the beam. The absolute polarization is given by normalizing against another polarimeter implemented at RHIC, namely a polarized hydrogen gas jet polarimeter. In this report, the details of polarization measurements, data analysis, and systematic uncertainties are discussed based on the data taken during $\sqrt{s} = 200$ GeV operation of Run05 at RHIC.

1 Introduction

The polarization of the proton beams [1] at the Relativistic Heavy Ion Collider (RHIC) is measured using both an atomic beam source hydrogen gas jet (H-Jet) [2–4] and proton-carbon (pC) polarimeters [5,6]. These polarimeters are set up in the 12 o'clock area (IP12) in the RHIC ring. The H-Jet polarimeter is located at the collision point allowing measurements of both beams. Two identical pC-polarimeters are equipped in the yellow and blue rings, where the rings are separated. The pC-polarimeter measures relative polarization to a few percent statistical accuracy within 20 to 30 seconds using an ultra-thin (typically $6\text{--}8 \mu\text{g}/\text{cm}^2$) carbon ribbon target, providing fast feedback to beam operations and experiments. Sufficient statistics also allows us to observe microscopic structures of the beam such as bunch by bunch basis polarizations and a polarization profile. The absolute normalization is provided by the H-Jet polarimeter, operated in parallel to pC polarimeters. Yet it accumulates much less statistics, i.e. takes over 1–2 days to obtain $\approx 5\%$ statistical uncertainty (as of Run05). The operation of pC polarimeters was thus focused on the better control of relative stability between one measurement to another rather than the polarization measurement in an absolute scale.

The published data of the analyzing power for the elastic polarized proton-carbon scattering is available up to the proton beam energy of 21.7 GeV/c [7]. There are no published data available at the storage (flat-top) proton beam energy of 100 GeV where the colliding experiment

^a e-mail: itaru@riken.jp

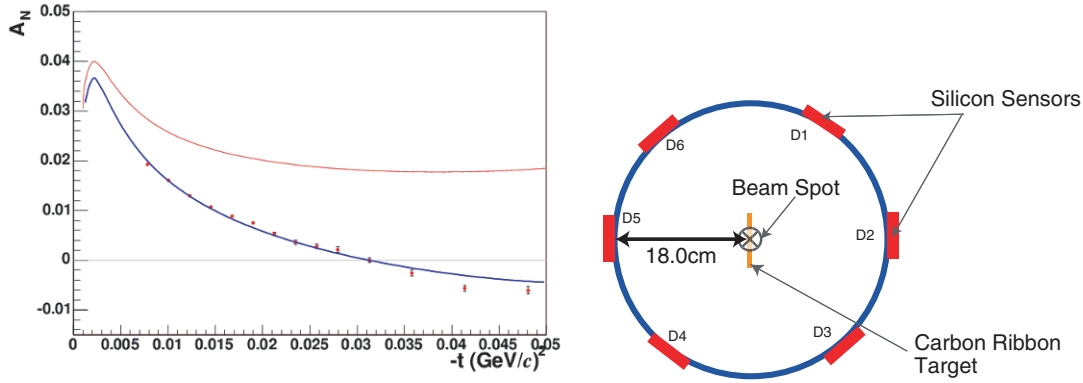


Fig. 1. Left: the analyzing power measured by the blue carbon polarimeter during Run04 for the extended range of the momentum transfers $-t$. The absolute scale was normalized against the hydrogen polarimeter results in Run04. Right: a cross section of the RHIC pC-polarimeter setup. Silicon sensors are aligned 45° , 90° , and 135° azimuthally in both left and right sides with respect to the beam direction. The beam points into the figure perpendicularly.

was performed in RHIC. Shown in the Fig. 1 is the analyzing power measured by the blue carbon polarimeter during Run04 operation for the extended range of the momentum transfers $-t$. The absolute scale was determined by normalizing the average polarization observed by the carbon polarimeter against the absolute polarization measurements by the hydrogen polarimeter in synchronized operation period. Although the shape of A_N as a function of $-t$ is well determined by the data with sufficient statistics accumulated by the pC polarimeter, the precision of the absolute scale was limited by the statistical accuracy of the H-Jet measurement;

$$\Delta A_N^{\text{Run04}} \approx \pm 9\%.$$

The strategy is to improve the accuracy year by year with more statistical abundance in the average polarization measurements by the carbon $P_{\text{pC}}^{\text{Run06}}$ and the hydrogen $P_{\text{H-Jet}}^{\text{Run06}}$ polarimeters. The improved analyzing power of Run06 A_N^{Run06} is given by

$$A_N^{\text{Run06}} = A_N^{\text{Run04}} \frac{\overline{P_{\text{pC}}^{\text{Run06}}}}{\overline{P_{\text{H-Jet}}^{\text{Run06}}}}. \quad (1)$$

The curves in the Fig. 1 are the model predictions [8] of with (blue) and without (red) the spin-flip amplitude fitted to the data. The analyzing power for the elastic polarized proton-carbon scattering is predicted to be maximized at the momentum transfer of $(-t \approx 0.003(\text{GeV}/c)^2)$ due to the interference between the electromagnetic and the strong amplitudes (this is known as the Coulomb-Nuclear Interference (CNI) region). In order to take advantage of relatively large sensitivity to the polarization, the recoil carbon atoms were detected near 90° degrees with respect to the beam direction to be as small t as possible. Kinetic energy range is selected from 400 to 900 keV, whose corresponding momentum transfer is $0.09 \leq -t \leq 0.23(\text{GeV}/c)^2$. The lower the kinetic energy, the larger the analyzing power and the more sensitivity we gain. The optimization of the energy range is the consequence of the trade off between the amplitude of the analyzing power and the reliability of the energy measurement of the low energy carbon ions. Details are discussed in Ref. [6]. Since there is a t -dependence in the analyzing power even within the limited t coverage, the relative energy of recoil carbon ion needs to be measured to define the kinematics. An alternative option to detect the forward scattered proton instead of the low energy recoil carbon ion is even more difficult because of the tiny transverse kick given by $-t$ in CNI region. The scattered proton goes too close to the primary beam and is unrealistic within the present divergence of the beam.

2 Experimental apparatus

The carbon polarimeters consisted of a carbon target and six silicon strip detectors. They are all mounted in the vacuum inside a scattering chamber.

Very thin carbon ribbon targets have been developed at Indiana University Cyclotron Facility [9]. The targets were made by vacuum evaporation-condensation onto smooth glass substrates. Typically size of 2.5 cm length with 6–8 $\mu\text{g}/\text{cm}^2$ thick and 10–20 μm width target was glued both edge on an open side of the “C”-shaped target folder frame. The targets are normally kept away from the beam line and it rotated into the beam only when the polarization measurement is executed, with a choice of 6 vertical and 4 horizontal targets for Run06. It is crucial to mount multiple targets simultaneously because the target is so thin, and has a certain lifetime against the radiation damage. The target lasted within a week on average and the pre-mounted spare target was used without breaking the vacuum to replace the broken one.

Six silicon sensors manufactured by the Instrumental Division at BNL were mounted in a vacuum chamber at 45, 90, 135 degrees azimuthally in both left and right sides with respect to the beam with schematic shown in right panel of Fig. 1. The sensor has $10 \times 24 \text{ mm}^2$ total active area, divided into 12 strips of $10 \text{ mm} \times 2 \text{ mm}$ each. The segmented axis of the detectors are oriented to the azimuthal direction, so there is no segmentation of the detectors in the beam direction. Thus the present setup do not have any sensitivity to the scattering angle of the recoil carbon ions within the acceptance. The thickness of the detector is $400 \mu\text{m}$, fully depleted with the operation bias voltage of 100 to 150 V. The strips are made by the Boron implantation p+-doping to a depth of 250 nm on the n-type Si bulk on the side facing the target. The distance from target to the silicon sensors was 18.0 cm.

3 Analysis

3.1 Asymmetries

Shown in the Fig. 2 left panel is the typical time-of-flight and the kinetic energy plot reconstructed. An energy correction is applied to the measured energy for the unmeasured energy loss in the surface region (“effective dead-layer”) of silicon sensors [6]. Solid curve represents 3σ cut on the invariant mass as demonstrated by dashed lines in right panel Fig. 2. The background tail towards smaller mass region is primarily comes from inelastic α s whose invariant mass does not necessarily be reconstructed at the right α mass because the energy loss in the effective dead-layer was calculated assuming the carbon ion. A contamination of the α backgrounds underneath the carbon invariant mass peak is typically much less than 1% within 3σ from the nominal carbon mass position. Within 3σ cuts, the number of the elastic carbons are observed about 200–300 thousand events. About 50% of accumulated events from raw data were dropped after the energy ($400 \leq E \leq 900$) and the 3σ cuts were applied.

The run-by-run polarization is calculated based on the strip asymmetries, combining all bunch-by-bunch asymmetries. The asymmetry of strip i is calculated using the number of elastic carbon events after the kinematic cuts for all positive bunches N_i^+ and negative bunches N_i^- in strip i :

$$A_i = \frac{N_i^+ - R_i N_i^-}{N_i^+ + R_i N_i^-} \quad (2)$$

where i runs for active strips up to 72. The luminosity ratio for the strip i is defined

$$R_i = \frac{\sum_{j \neq i, 37-i, 36+i, 72-i}^{72} N_j^+}{\sum_{j \neq i, 37-i, 36+i, 72-i}^{72} N_j^-}. \quad (3)$$

Shown in Fig. 3 with solid circles are typical example of strip asymmetries divided by the $\overline{A_N}$ plotted as a function of the azimuthal angle of each strip in the unit of radian. The coverage of the 2 mm strip width is translated to be 11 mrad in the azimuthal angle acceptance.

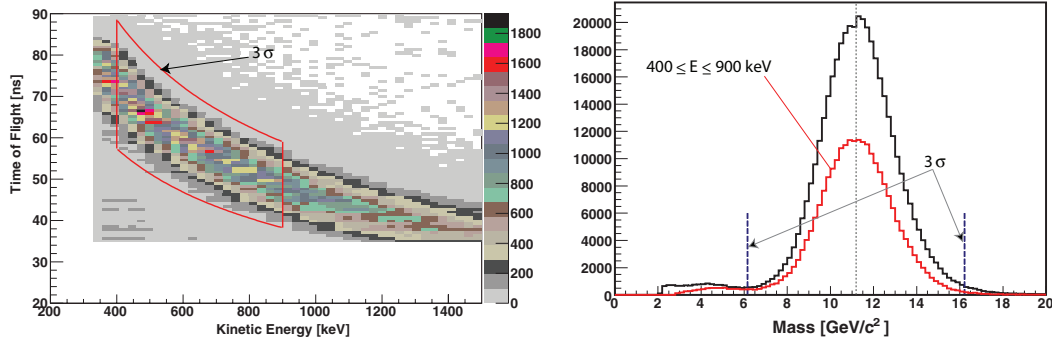


Fig. 2. Left: time of flight and reconstructed kinetic energy correlation plot after the energy correction. Solid curve distinguishes events within 3σ from carbon mass in the invariant mass distribution and the energy range $400 \leq E \leq 900$ keV. Right: a typical reconstructed invariant mass distribution. The red histogram shows the invariant mass for the events $400 \leq E \leq 900$ keV whereas black histogram all events in a given strip. Dashed line represents 3σ from the nominal carbon mass (dotted line).

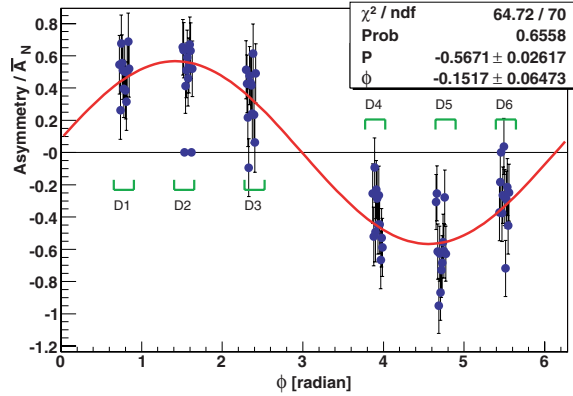


Fig. 3. The strip by strip polarization plotted as a function of the azimuthal angle (rad). The red curve represents the best fit to the data of function 4.

The strip by strip polarizations are then fitted with the sine function

$$P(\phi) = \frac{A_i}{\overline{A_N}} = P \sin \phi \quad (4)$$

where P is strip averaged polarization, ϕ is the radial polarization vector, and $\overline{A_N}$ is cross section weighted average A_N , respectively. P and ϕ were set as free parameters. The best fit result is drawn by the solid curve in the figure.

3.2 Polarization profile

The typical beam size at the 100 GeV at the location of pC polarimeters is around 1.5–2 mm at FWHM, while the carbon ribbon target width is only 4–10 μm . Thus it measures only the local polarization of the beam wherever the target is positioned with respect to the beam. On the other hand, the FWHM of the H-Jet gas target is about 6 mm, wide enough to cover the whole beam spot size at IP12. Therefore what the H-Jet measures is averaged polarization over the beam polarization profile. The intrinsic difference between pC and the H-Jet polarimeters is thus the coverage area of the finite transverse target beam spot size as illustrated in Fig. 4. Yet the measured polarization by pC-polarimeters can be directly comparable to what the H-Jet polarimeter measures and applicable to the experiments, if there is

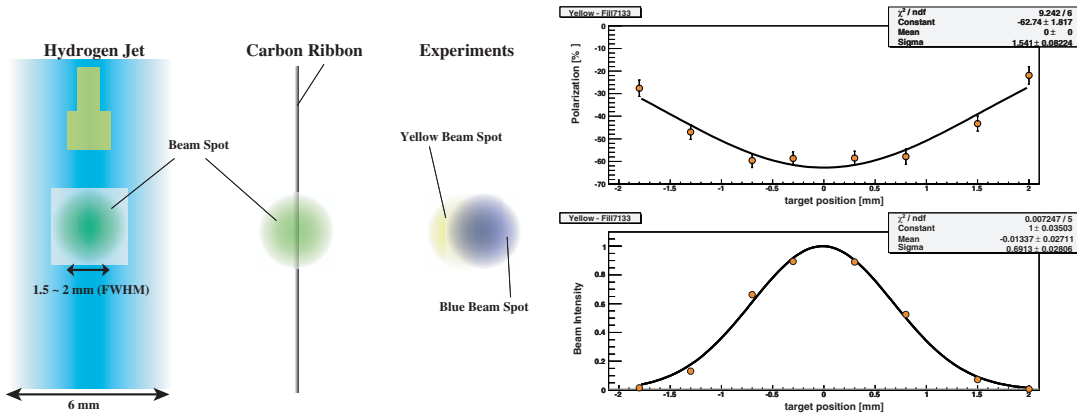


Fig. 4. Left: images of the area coverage difference of the target on the beam spot between the H-Jet and proton-Carbon polarimeters and experiments from left, respectively. Right: the horizontal polarization (top) and the intensity (bottom) profiles of the yellow beam observed during Run05. The vertical axis of the intensity profile is calculated from the event rates normalized at the peak amplitude of the Gaussian fit. The horizontal axes are the relative target position in mm with respect to the beam center defined by the Gaussian fit on the intensity profile.

no polarization profile in the beam. In reality, the RHIC beam often show finite polarization profiles.

Shown in right panel Fig. 4 are the polarization (top) and intensity (bottom) profiles observed during one of a fill in the yellow ring during Run05. Each data point corresponds to an independent polarization measurement at a given target position with respect to the beam. Series of measurements were executed until the scan in every ≈ 0.5 mm step across the horizontal beam profile was completed. Despite the event rate dropped so rapidly toward the edge of the beam, each measurement was accumulated constant statistics, i.e. ≈ 20 M events to well define the both wings of the profile. As figures demonstrate, both polarization and intensity profiles were well fit by the Gaussian shape. The strength of the profiles can be characterized by the widths σ .

The two Gaussians of the beam intensity and the polarization profiles are given as a function of the target position x (x is the distance from the intensity peak, not absolute target position):

$$\mathcal{I}(x) = e^{-\frac{x^2}{2\sigma_I^2}} \quad (5)$$

$$\mathcal{P}(x) = e^{-\frac{x^2}{2\sigma_P^2}} \quad (6)$$

where $\mathcal{I}(x)$ and $\mathcal{P}(x)$ are the intensity and polarization profiles normalized to be 1 at their peaks, and σ_I and σ_P are width of these profiles, respectively. There are also profiles in vertical direction, but it is averaged over for this case. Eliminate x from these equations, then we obtain

$$\mathcal{P} = \mathcal{I}^{r_x} \quad (7)$$

where

$$r_x = \left(\frac{\sigma_I}{\sigma_P}\right)^2. \quad (8)$$

Since \mathcal{I} and \mathcal{P} are defined as the relative intensity and the polarization with respect to the peak, they run from 0 to 1. Thus Eq. (7) gives $\mathcal{P} = 1$ at the peak intensity $\mathcal{I} = 1$.

The correction enforced due to the polarization profile applied for polarizations measured by pC polarimeters in fact affected a large impact on the precision of Run05 polarizations. There performed only three dedicated measurements as Fig. 4 throughout Run05, poor knowledge about the profile resulted in large uncertainty in its correction. The polarization

profile correction actually dominated the systematic error of the normalization process against the H-Jet polarimeter [6]. In Run06, such a correction was avoided by scanning the carbon wire target across the transverse beam profile for every measurements. Since the vertical (horizontal) wire target automatically averages over one dimension, scanning over horizontal (vertical) direction during the measurement averages over another dimension. As a consequence the average polarization measured by the pC polarimeter in so called “scan mode” literary emulates the average polarization measured by the H-Jet polarimeter without applying any polarization profile corrections. The scan was made with several hundred μm steps across the beam intensity profile for a constant intervals (typically a few seconds) at each target position.

3.3 Normalization

The H-Jet polarimeter was operated for the blue and yellow beams sequentially switching every a couple of days or so during Run06. We grouped these H-Jet operation period and compare with the polarizations of pC polarimeters averaged over the corresponding periods, respectively. Whereas the H-Jet polarimeter was operated continuously throughout a fill, pC polarimeters take only a “snapshot” polarization of the fill multiple times (typically 4 or 5 times for 7 hours fill). As well as transverse polarization profile, the H-Jet polarimeter also averages the polarization over the fill. As a consequence, the measured polarization is automatically biased by the period while the beam intensity is high simply because it triggers more events to the H-Jet polarimeter. On the other hand, each measurement of pC polarimeters was accumulated same statistics regardless of the beam intensity. Thus the polarizations were calculated by taking weighted average by the beam intensity for pC polarimeters.

Shown in Fig. 5 are the ratio of the average polarizations of pC and H-Jet polarimeters. Linear fits shown in solid lines give $\chi^2/d.o.f$ of 6.3/4 and 1.1/2 for the blue and the yellow average polarizations, respectively. The Run06 absolute normalization scales $S = \overline{P_{\text{pC}}^{\text{Run06}}} / \overline{P_{\text{H-Jet}}^{\text{Run06}}}$ for pC polarimeters determined by the fit were 1.138 ± 0.030 and 1.152 ± 0.026 for the blue and yellow polarimeters, respectively. Errors are statistical only, which primarily come from the average polarizations of the H-Jet polarimeter.

Global errors [10], which are correlated from fill to fill are estimated and summarized in Table 1. The total of global uncertainties are given by the quadratic some of each global errors. Besides global correlated errors, uncorrelated errors which applies to the average polarizations fill by fill, are estimated 1.2% as the energy correction, and 2.0% as the vertical profile uncertainties. The latter is originated from short of vertical profile measurements throughout Run06 and calculated from the the possible range in r_y from a maximal variation ($\pm\text{RMS}$) from mean values of r_x ($(0.071 + 0.094)/2$) of the blue and yellow beams: 0.085 ± 0.085 . This range was considered as a possible range in the average over fills vertical profile as well as possible fill

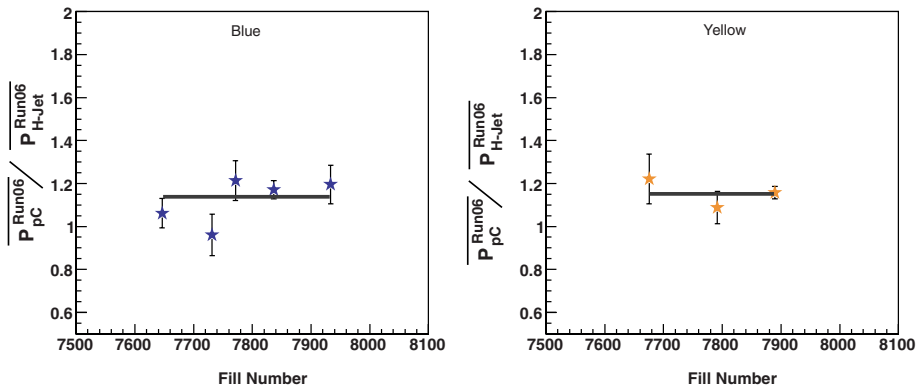


Fig. 5. The ratio of the average polarizations measured by the pC and the H-Jet polarimeters for several periods of the blue (left) and the yellow (right) beams. Solid lines are linear fits to data.

Table 1. The global systematic uncertainties.

Errors	Blue ($\Delta P_B/P_B$)	Yellow ($\Delta P_Y/P_Y$)
Normalization Statistical	2.3%	2.4%
Normalization Horizontal Profile	1.1%	1.1%
Normalization H-Jet Molecular Contamination [3,4]	2.0%	2.0%
Normalization H-Jet Other systematic [3,4]	1.3%	1.5%
Polarization Profile for Experiments	2.0%	2.0%
Energy Correction	2.4%	2.4%
Total	4.7%	4.8%

from fill fluctuation in vertical profile. Resulting global systematic errors are estimated to be 4.7% and 4.8% for blue and yellow beams, respectively.

4 Summary

In summary, the proton-carbon polarimeters were developed to measure the polarization of the polarized proton beams at RHIC. The left-right asymmetry of recoil carbon events through the elastic proton-carbon reaction provides polarization of the proton beam in a relative scale. The absolute scale is given by normalizing the average polarization of given period measured by the pC polarimeter against that of H-Jet polarimeter operated for the same period. Using an ultra-thin carbon ribbon target, the polarization measurement with a few percent statistical accuracy can be done within 20 to 30 seconds, providing fast feedback to the beam operation and experiments. pC polarimeters also provide detailed structures of the polarized beam by evaluating the polarization in bunch by bunch basis, mapping out the polarization profile across the beam. Such a portability plays important role for the accelerator tuning at RHIC. As a result of careful offline analysis, the global systematic errors of 4.7% and 4.8% for the average polarization in the blue and the yellow beams, respectively were achieved in Run06. The dominant uncertainty of which associated with the vertical polarization profile primarily due to short of measurements.

References

1. I. Alekseev, et al., Nucl. Instrum. Meth. A **499**, 392 (2003)
2. A.N. Zelenski, et al., Nucl. Instrum. Meth. A **536**, 248 (2005)
3. H. Okada, et al., Phys. Lett. B **638**, 450 (2006)
4. K.O. Eysler, et al., RHIC/CAD Acceler. Phys. Note, **274** (2007)
5. O. Jinnouchi, et al., RHIC/CAD Acceler. Phys. Note, **171** (2004)
6. I. Nakagawa, et al., RHIC/CAD Acceler. Phys. Note, **275** (2007)
7. J. Tojo, et al., Phys. Rev. Lett. **89**, 052302 (2002)
8. L. Trueman (2003) [[hep-ph/0305085](#)]
9. W.R. Lozowski, J.D. Hudson, Nucl. Instrum. Meth. A **303**, 34 (1991); Nucl. Instrum. Meth. A **334**, 173 (1993)
10. I. Nakagawa, et al., Nucl. Instrum. Meth. (submitted)